Numerical Prediction of Rotor Tip-Vortex Roll-Up in Axial Flights by Using a Time-Marching Free-Wake Method

Ki-Hoon Chung*, Seon-Uk Na, Wan-Ho Jeon** and Duck-Joo Lee*****
Division of Aerospace Engineering, Department of Mechanical Engineering, KAIST, 373-1, Yusong-Gu, Kusong-Dong, Taejon, 305-701, KOREA

Abstract

The wake geometries of a two-bladed rotor in axial flights using a time-marching free-wake method without a non-physical model of the far wake are calculated. The computed free-wake geometries of AH-1G model rotor in climb flight are compared with the experimental visualization results. The time-marching free-wake method can predict the behavior of the tip vortex and the wake roll-up phenomena with remarkable agreements. Tip vortices shed from the two-bladed rotor can interact with each other significantly. The interaction consists of a turn of the tip vortex from one blade rolling around the tip vortex from the other. Wake expansion of wake geometries in radial direction after the contraction is a result of adjacent tip vortices begging to pair together and spiral about each other. Detailed numerical results show regular pairing phenomenon in the climb flights, the hover at high angle of attack and slow descent flight too. On the contrary, unstable motions of wake are observed numerically in the hover at low angle of attack and fast descent flight. It is because of the inherent wake instability and blade-vortex-interaction rather then the effect of recirculation due to the experimental equipment.

Key word: Roll-Up, Rotor Wake, Time-Marching Free-Wake, Slow Starting Rotation, Parabolic Blending Method

Introduction

The tip vortices are one of the most significant but poorly understood aerodynamic features of a helicopter rotor wake. In contrast to fixed-wing aircraft where the tip vortices trail downstream, rotor tip vortices can remain in close proximity of the rotor for a significant amount of time. They are key factors in determining the rotor performance and local blade loads. Under many flight conditions, especially during maneuvers and descent flights, the blades interact closely with the tip vortices resulting in a phenomenon known as Blade-Vortex-Interaction (BVI).

Currently available methods of wake analysis of helicopter flow fields range from relatively simple momentum theory to lifting-surface methods with wake modeling[1,2]. The difficulties of lifting-surface methods, in describing the stall and shock for retreating and advancing blade respectively, has led to recent efforts on using computational fluid dynamics (CFD) codes[3,4]. Basically the CFD codes can describe the generation and the movement of the vorticity in the wake. However, the inherent numerical dissipation causes a rapid decay of the vortical structures. Another problem occurring in the use of CFD codes is the far wake boundary condition especially for hovering flight, which condition should be carefully implemented also in the free-wake analysis.

* Ph.D. Candidate
** Post Doctoral Fellow
*** Professor

Traditionally, the prescribed wake model[5,6], an iterative free-wake model[2,7,8,9], and a time-marching, free-wake model[1,10] have been successfully used to calculate the blade loadings and wake structures in certain conditions. However, more realistic wake geometry, which describes the overall regions of the wake including the far wake, has not been attempted properly. Whether iterative or time-marching free-wake methods, the far-wake model and the artificial initial wake condition should be employed to obtain a converged steady solution in hover using the previously developed methods. Typically, the far wake is modeled by a vortex ring[7] or a semi-infinite cylinder[8]. The far wake may also be truncated after several spirals of the wake[11]. The initial state of wake is critical, especially for the time-marching method, because the instability of the wake exists due to the strong starting vortex generated with the assumption of an impulsively rotating blade. Therefore, a helicoidally spiral wake is used initially[11] or a uniform axial velocity[12] is superposed for the impulsively rotating condition. These methods enable the movement of the initial vortex wake downward from the rotor disk to avoid problems of instability during the initial stage. However, the true transient solution and the wake evolution mechanism cannot be predicted.

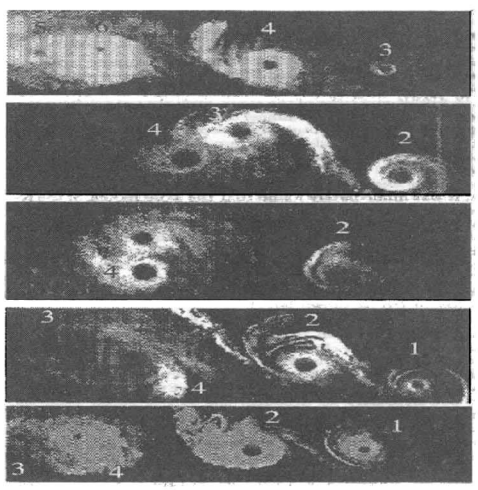

Fig. 1. Sequence of vortex roll-up from the individual blade, 9 degree collective, 3.5 fps climb rate (Caradonna et al and Komerath et al [13])

Recent experiments[13] shows that the tip vortices shed from a two-bladed rotor could interact significantly. The interaction consists of a turn of the tip vortex from a blade rolling around the tip vortex from the other. The wake does not contract monotonically but expands as one of the vortices moves radially outward due to the roll-up. The hovering rotor wake can be represented by three regions based on previous experimental visualization: a well-defined tip vortex contraction region, an intermediate wandering region, and an initially generated far wake bundle. The well-defined 3~4 tip vortices have been properly correlated from experimental data and reasonably predicted by numerous methods[4,5,6,8]. Recently, computations of the intermediate wandering region have been attempted to simulate the motion of the tip vortices using Adams-Moulton method to advance the vortices and modified Biot-Savart law to describe the vortex structure[14]. But the computation has only achieved the primary goal of demonstrating that the roll-up phenomenon is intrinsic to rotor wake and should not be ignored. The accurate prediction of the rotor-wake geometry is not satisfied yet.

Fig. 1 shows a sequence of images of the tip vortex development at a rotor collective angle of 9^o and climb rate of 3.5 fps[13]. The vortices from the two blades are identified by their numbers, i.e. an odd numbered vortex belongs to one blade and even numbered to the other. The time spacing between each successive frame is not constant, but it is chosen to show the progress of the pairing phenomena. The first frame shows two clear vortices, marked '3' and '4'. In the next frame, vortex '3' has begun to roll up with '4'. This process continues in the next two frames, until '3' and '4' have essentially interchanged their positions while moving downstream (left direction in Fig. 1). The notable aspect of this visualization is that the vortex trajectories do not appear to follow a path whose contraction increases monotonically with time. Beyond a certain age, the vortex trajectory tends to expand radially (downward direction in Figure 1). Moreover, the spacing between the tip vortices seems to change. Such vortex expansion have been noted in many previous tests and visualizations, and frequently attributed to being some manifestation of an unstable process. However, the vortex expansion was seen to be a result of adjacent tip vortices beginning to pair together and spiral about each other[13].

In this paper, a real time-marching free-wake method is described, which does not require the non-physical initial condition and the far-wake model. And the mechanism of the intermediate unsteady region can be explained, which might be very important in predictions of unsteady loads and noise in certain flight conditions. The wake geometries generated by model AH-1G rotor with 41-inch radius are predicted and the results are compared with experimental wake roll-up visualization data[13]. These objectives can be fulfilled, not only by using the accurate numerical scheme, but also by observing the physical phenomena carefully. One of the key points is that the rotation speed must be increased slowly from zero to the required speed[15,16,17], a factor that has been overlooked by most previous researchers. The curved vortex filament should be integrated carefully to obtain the induced velocity. This is well proved for the elliptic vortex roll-up[18]. The far wake is automatically produced as the blades are rotating slowly without the non-physical far wake model. Three conditions of flight; climb, hover and descent, are calculated with the time-marching free-wake method, which show stable or inherent unstable conditions of wake roll-up.

Formulation

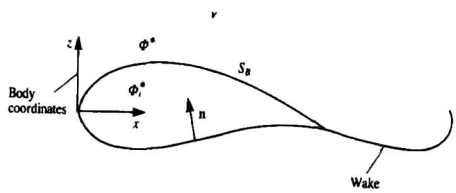

Fig. 2. Potential flow over a closed body

The fluid surrounding the body is assumed to be inviscid, irrotational, and incompressible over the entire flow field, excluding the body's solid boundaries and its wakes as shown in Fig. 2. Therefore, a velocity potential $\Phi(\vec{x}, t)$can be defined and the continuity equation in the inertial frame becomes:

$$\nabla^2 \Phi = 0 \tag{1}$$

The boundary condition requiring zero normal velocity across the body's solid boundaries is:

$$(\nabla \Phi + \vec{V}_{wake} - \vec{V}) \cdot \vec{n} = 0 \tag{2}$$

Where $\vec{V}_{wake}(\vec{x}, t)$ is the induced velocity due to the vorticity field in the wake, $\vec{V}(\vec{x}, t)$ is the body surface's velocity, and $\vec{n}(\vec{x}, t)$ is the vector normal to the moving surface, as viewed from the blade. Using Green's second identity, the general solution of equation (1) can be constructed by integrating the contribution of the basic solution of source(σ) and doublet(μ) distributions over the body's surface:

$$\Phi(\vec{x}, t) = \frac{1}{4\pi} \int_{body+wake} \mu \vec{n} \cdot \nabla(\frac{1}{r}) ds - \frac{1}{4\pi} \int_{body} \sigma(\frac{1}{r}) ds \tag{3}$$

Inserting equation (3) into equation (2) becomes:

$$\left\{ \frac{1}{4\pi} \int_{body+wake} \mu \nabla [\frac{\partial}{\partial n}(\frac{1}{r})] ds - \frac{1}{4\pi} \int_{body} \sigma \nabla(\frac{1}{r}) ds - \vec{V} \right\} \cdot \vec{n} = 0 \tag{4}$$

The source term is neglectable in the case of thin blades. Thus, only the first part of equation (3) is used to represent the lifting surface. The constant-strength doublet panel is equivalent to a closed vortex lattice with the same strength of circulation ($\Gamma = \mu$). Then the induced velocity of the vortex lattice in equation (4), representing the blade, can be obtained by using Biot-Savart's Law:

$$\vec{V} = -\frac{1}{4\pi} \int_c \frac{\vec{r} \times \Gamma \vec{dl}}{|\vec{r}|^3} \tag{5}$$

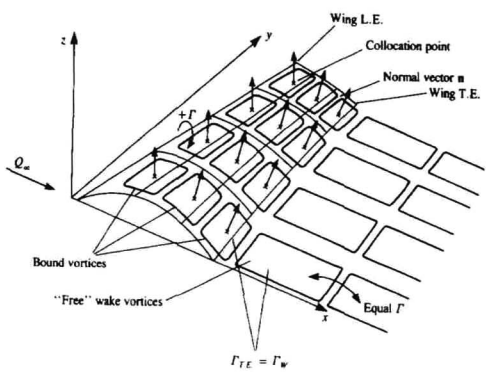

Fig. 3. Vortex model for a thin lifting surface

The collocation point is at the mid-span and three-quarter chord of each lattice as show in Fig. 3. The boundary condition of no-flow penetration is satisfied at the collocation point of each lattice. The application of the flow tangency condition(equation (4)) to the vortex lattice distribution yields the following linear matrix equation that is to be solved:

$$A_{ij}\Gamma_j = R_i \quad (i, j = 1, n) \tag{6}$$

where A_{ij} id the coefficient matrix of normal induced velocity on the i-th element of the blade due to the j-th vortex lattice with the unit circulation, and Γ_j is the unknown circulation value of the blade vortex lattice. R_i is the normal induced velocity at each control point due to the free stream velocity, the blade-moving velocity, and the wake-induced velocity.

Time-Marching Free-Wake Method

A three-dimensional wing trails the bound circulation(Γ) into the wake. Radial variation of bound circulation produces trailed vorticity in the wake, which direction is parallel to the local free stream direction at each instant it leaves the blade. Azimuthal variation of bound circulation produces shed vorticity, oriented radially in the wake. The strength of the trailed and shed vorticity are determined by the radial and azimuthal derivatives of bound circulation at the time wake element leaves the blade. The bound circulation has a peak near the tip, and quickly drops to zero. The trailed sheet therefore has a high strength(proportional to the radial derivative of Γ) at the outer wake, and quickly rolls up into a concentrated tip vortex. The strength of the trailed shed wake vortex at this time step is set equal to the one of the vortex lattice elements, which is located at the trailing edge of the blade ($\Gamma_{T.E,t} = \Gamma_{wake,t}$). This condition is forced to satisfy the Kutta condition($\gamma_{T.E} = 0$) .

Since the wake surface is force-free, each vortex wake element moves with the local stream velocity, which is induced by the other wake element and the blades. The convection velocity of the wake is calculated in the inertial frame. The vortex wakes are generated at each time step. Therefore, the number of wake-elements increases as the blade is rotating. It is clear that a large number of line elements for highly curved and distorted wake region like the tip vortex are necessary to describe the vortex filament distortions accurately. In general, computational time for the calculation of the wake distortion is proportional to the square of the vortex element number. Therefore, the curved element is used for a small number of elements.

There are many mathematical expressions to represent the three dimensional curves. Generally, cubic spline curves are used to describe the curves. However, the cubic spline curves have certain disadvantages; the cubic spline curves require a large tri-diagonal matrix inversion, and the numerical disturbance of position in any one segment affects all the global curve segments. Therefore, the curve is not adequate to represent the vortex filament motion in strong interaction problems. The parabolic blending curves, employed here, maintain the continuity of the first derivative in space, which is critical to our problem. The parabolic blending curve, $C(\zeta)$, is given by

$$c(\zeta) = (1 - \zeta)p(r) + \zeta q(s) \tag{7}$$

The function of $p(r)$ and $q(s)$ are parametric parabolas through P_1, P_2, P_3 and P_2, P_3, P_4 as shown in Fig. 4, respectively. A generalized parametric blending curve is developed from the assumption of normalized chord length approximation for the position parameter, r and s at P_2 and P_3 which are linearly related with the parameter ζ respectively, *i.e.* $0 \le r, s, \zeta \le 1$. Then we apply this blending curve to equation (5).

which is formulated by Moore-Rosenhead[19,20]. It is defined as

$$\vec{V} = \frac{1}{4\pi} \int_c \frac{\vec{r}}{(|\vec{r}|^2 + \mu^2)^{3/2}} \times \Gamma \frac{\partial y(\zeta, t)}{\partial \zeta} d\zeta \tag{8}$$

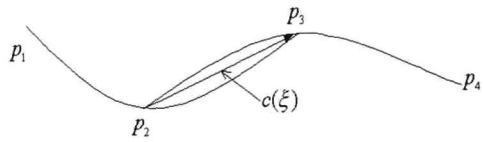

Fig. 4. Parabolic blending method

Here $y(\zeta, t)$ is the position vector of a material point denoted by Lagrangian variable ζ at an instance, which describes cut-off parameter μ is used to remove the singularity problem in the Biot-Savart's law at the region very closed to the vortex filaments.

The impulsive rotation method of free wake calculation causes non-physical strong instability of the initial wake. So the wake becomes unstable after a few spirals of the wake as shown in Fig. 5.

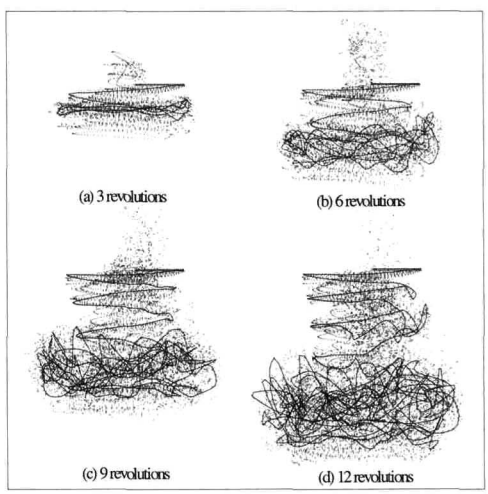

Fig. 5. Wake geometry of impulsively rotating case for a one-bladed rotor

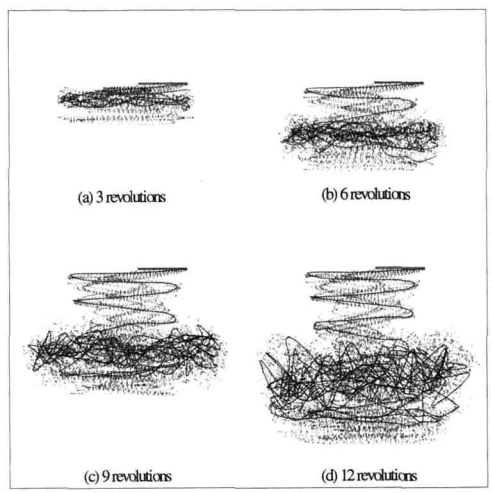

Fig. 6. Wake geometry of slowly starting case for a one-bladed rotor

One of the key points to overcome these non-physical phenomena is that the rotation speed must be increased slowly from zero to the required speed. This approach is critical to the curved vortex filament for the simulation of rotor wake [15,16,17]. Fig. 6 shows that the strength of the initial wake is weak for the slowly starting case, the instability of wake is suppressed, and the wake moves downward slowly where the far wake is automatically produced.

Tip Vortex Geometry Calculation

In this approach, no physical assumption is made about the roll-up of inner wake sheet. It is theorized that the computation of the lattice convection is able to correctly predict the roll-up of inner wake sheet and the tip vortex concentration[16,17]. The sheet influence on the load is introduced by the velocity field induces by all of the filaments of the vortex lattice. No distinction is made between the inner and outer filaments that are thus considered to be potential interacting vortices.

The trajectories of tip vortex are re-calculated based on the results of the time-marching free-wake analysis (circulation Γ and location x, y, $z$of the trailedwakefilaments). The circulation Γ_t and location x_t, y_t, z_t of the tip vortex are calculated using the following procedure. The circulation Γ_t of tip vortex at each time step is obtained by summing up the circulation strength of outside trailed vortices at the maximum point over a spanwise portion along the blade:

$$\Gamma_t = \sum_{i=i_{max}+1}^{i=i_{tip}} \Gamma_i \tag{9}$$

where i_{max} is the index of the maximum lifting point and i_{tip} is that of rotor tip. The radial location r_t of the constructed tip vortex is calculated by using the following barycenter rule:

$$r_t = \left(\sum_{i=i_{max}+1}^{i=i_{tip}} \Gamma_i r_i \right) / \left(\sum_{i=i_{max}+1}^{i=i_{tip}} \Gamma_i \right) \tag{10}$$

The trajectory $z_t(t)$ of the tip vortices is obtained by using the barycenter rule defined previously for the computation of r_t:

$$z_t = \left(\sum_{i=i_{max}+1}^{i=i_{tip}} \Gamma_i z_i \right) / \left(\sum_{i=i_{max}+1}^{i=i_{tip}} \Gamma_i \right) \tag{11}$$

Results

The rotor used in this wake calculation is AH-1G's 41-inch radius model rotating at 1800 rpm. The blade is modeled using five chordwise panels and ten spanwise panels. This rotor is the same as that used in the experiments of Caradonna et al and Komerath et al[13]. Twenty-four time-steps are taken per blade revolution and the vortex core radius is taken as 10% of the chord length. The tip-vortex pairing process has been quantified by using the trajectory tracking method.

Tip-vortex roll-up mechanism

The trajectories of the tip-vortices, which are calculated by using time-marching free-wake method, are shown in Fig. 7. The left figure shows the three-dimensional view of tip vortex trajectories and the right one shows the cross section view of that.

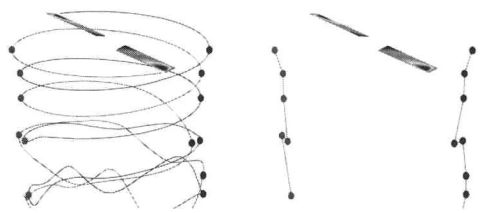

Fig. 7. 3D view and cross section view of wake

Fig.8 shows the tip-vortex roll-up process for collective angle of 11^{o} at a climb rate of 9.6 fps. In this figure, vortex '3' begins to roll up with '4'. This process continues until '3' and '4'

interchange their positions while moving downstream. We can clearly see that tip-vortex roll-up consists of a turn of the tip-vortex from one blade rolling around the tip-vortex from the other blade as shown in Fig. 1 even though Fig. 1

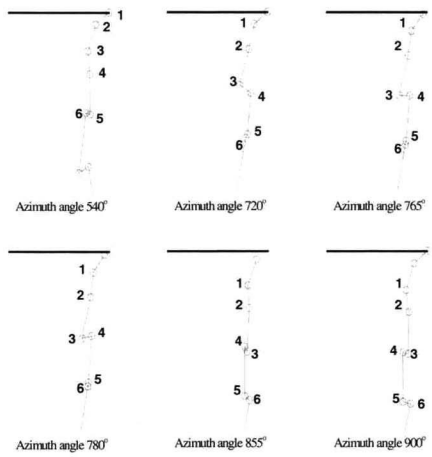

Fig. 8. Tip-vortex roll-up process at 11 degree collective angle, 9.6 fps climb rate

Comparison with experimental data

The trajectories of the tip vortices for collective angle of 6^o at a climb rate of 3.5 fps are shown in Fig. 9.

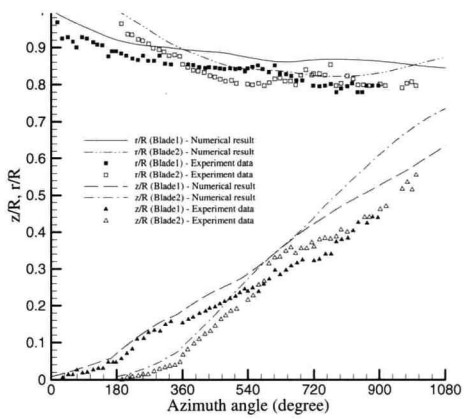

Fig. 9. Wake geometries at 6 degree collective angle, 3.5 fps climb rate

The tip vortex trajectories from the two blades are offseted by 180^o and it is clear that they are influencing each other. The first intersection of the z/R (axial direction) curves of the two vortices

indicated the beginning of the vortex pairing process. In this case the results of time-marching free-wake method has a little error about radial(r) and downstream(z) distance positions but shows that the tip vortex roll-up occurs at 610^{o}, which is the same as the experimental data.

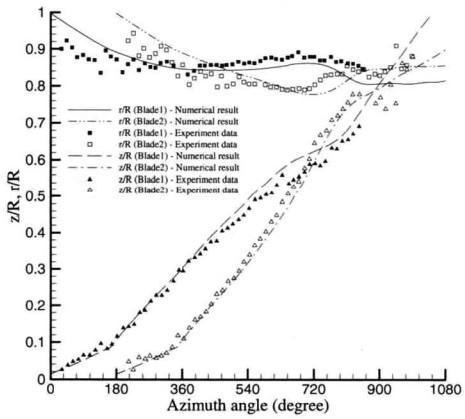

Fig. 10. Wake geometries at 11 degree collective angle, 3.5 fps climb rate

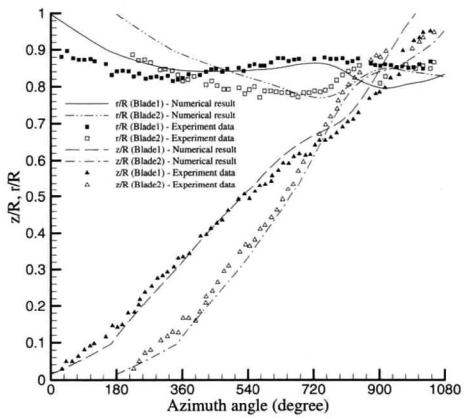

Fig. 11. Wake geometries at 11 degree collective angle, 9.6 fps climb rate

Fig. 10 shows the tip-vortices trajectories for higher collective angle of 11^{o} at the same climb rate of 3.5 fps. These trajectories clearly show that the local radial expansion is occurred by the result of adjacent tip vortices begging to pair together and spiral about each other. Subsequent crossings indicate the rotation of the two vortices about each other. A comparison of 6^{o} and 11^{o} case clearly shows that the initiation of the wake roll-up is delayed by increasing the collective angle from 610^{o} to 720^{o}. Fig11. shows the tip-vortices trajectories for collective angle of 11^{o} at a faster climb rate of 9.6 fps. These trajectories do not show significant differences compared with those in Fig. 10 since the effective inflow rates mostly influenced by the collective angle rather than the climb rate in these cases.

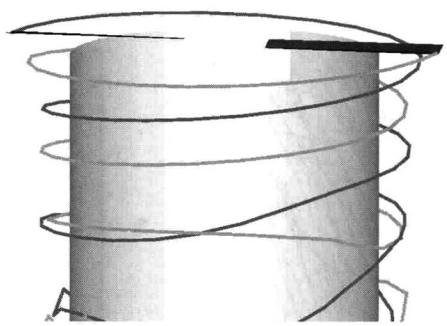

Fig. 12. 3-D tip vortex geometry at 11 degree collective angle, 9.6 fps climb rate

The computed wake geometries show excellent agreements with the experimental data as the higher collective angle. The three-dimensional wake trajectories calculated by using time-marching free-wake method at collective angle of 11^{o} and climb rate 9.6 fps are represented in Fig. 12. The crossing of the two tip vortices indicates the commencement of the roll-up process.

Instability of wake roll-up

Fig. 13 shows detailed view of tip-vortices geometries generated by two blades during 35 revolutions for collective angle of 11^{o} at hover flight. As initial wakes move to far downstream area, the tip-vortex roll-up converges to a certain steady state condition.

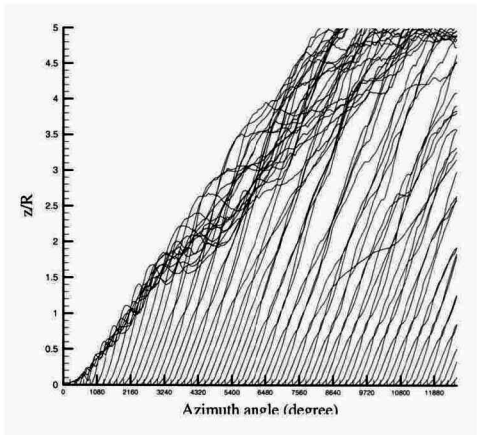

Fig. 13. Detailed tip vortex geometry during 35 revolutions at 11 degree collective angle, at hover flight.

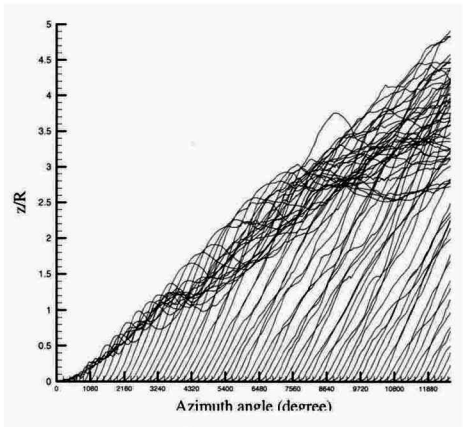

Fig. 14. Detailed tip vortex geometry during 35 revolutions at 6 degree collective angle, at hover flight

But Fig. 14 shows unstable state of wake roll-up in hover flight for 6^{o} collective angle. It is important to note that this instability is not a manifestation of a numerical instability. This flow unsteadiness seen in hover testing has been reported by Leishman and Bagai[21]. This shows that flow unsteadiness is occurred not only by the recirculation and the wind effect of the experimental condition but also by the inherent wake instability.

The tip-vortex geometries at 11^{o} collective angle with 3.5 fps climb rate during 35 revolution also show the steady state of wake roll-up as shown in Fig. 15.A comparison of Fig. 13 and Fig. 15 dose not bring put significant difference but Fig. 15 shows faster convergence to a certain steady condition.

Fig. 16 shows the tip-vortex geometries at 11^{o} collective angle with 3.5 fps descent rate during

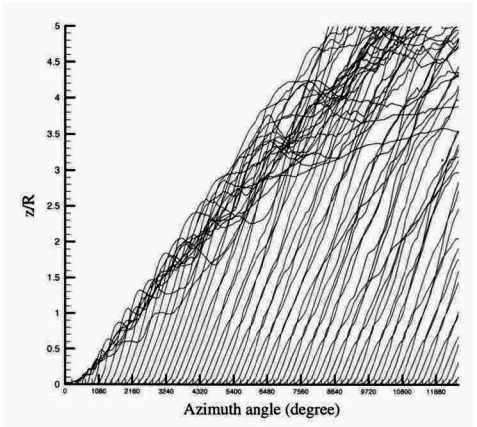

Fig. 15. Detailed tip vortex geometry during 35 revolutions at 11 degree collective angle, 3.5 fps climb rate

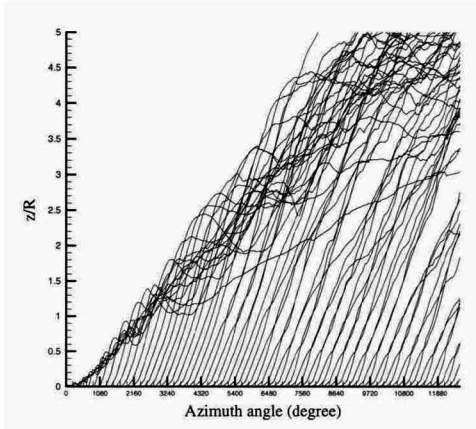

Fig. 16. Detailed tip vortex geometry during 35 revolutions at 11 degree collective angle, 3.5 fps descent rate

35 revolutions. In this case, wake roll-up converges to a certain steady state condition and the converged roll-up point is located to more closer to the rotor plane (z/R=0) than that of hover and climb case.

In Fig. 17, the tip-vortex geometries at 11° collective angle with faster 9.6 fps descent rate

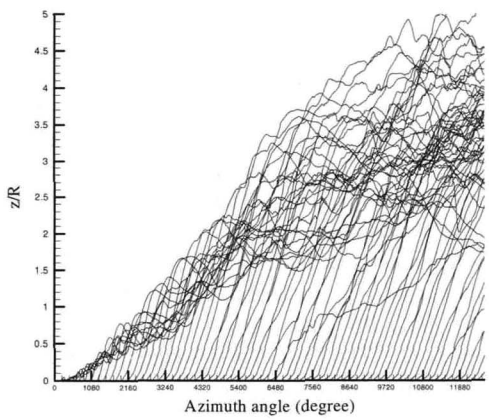

Fig. 17. Detailed tip vortex geometry during 35 revolutions at 11 degree collective angle, 9.6 fps descent rate

during 35 revolutions show the unstable state of wake roll-up. These random motion of the tip-vortices are due to the blade vortex interaction in addition to the instability of the wake.

Conclusions

The ability to predict the performance and aeroacoustics of the entire vehicle is strongly dependent on the ability to predict the highly interactive aerodynamics of the rotor wake. While considerable effort has been invested in the rotor wake problem, computational method, which can handle highly interactive rotor wake problem, has not yet been reported.

In this paper, the radial and axial geometries of the tip vortices are calculated without a far-wake model by using time-marching free-wake method. The time-marching free-wake method can predict the behavior of tip vortex and wake roll-up phenomenon with remarkable agreements. The computed wake geometries show excellent agreements with the experimental data. These excellent agreements can be achieved by using a slow starting rotor based on the physical phenomena.

Generation mechanisms of the wake roll-up are clearly understood from the free-wake calculations. Tip vortices shed from a two-bladed rotor can interact significantly and the interaction consists of a turn of the tip-vortex from one blade rolling around the tip-vortex from the other blade. The wake expansion is a result of adjacent tip vortices beginning to pair together and spiral about each other. The initiation of the wake roll-up is delayed by increasing the collective angle. The wake trajectories do not show significant differences in these ranges of climb rate change. Detailed numerical results show that a regular vortex pairing phenomenon in the climb flight, the hover at high angle of attack and slow descent flight. Random motions of the tip vortices are observed for the hover at low angle of attack due to the inherent wake instability and for the fast descent flight mainly due to the blade vortex interaction.

References

1. Baron, A., Boffadossi M., "Unsteady Free Wake Analysis of Closely Interacting Helicopter Rotors," Proc. 19th Eur. Rotorcraft Forum, Cernobbio (Como), Italy, Sept. 14-16, 1993.

2. Felker, F .F., Quackenbush, T .R., Bliss, D .B., and Light, J .L., "Comparisons of Predicted and Measured Rotor Performance Using a New Free Wake Method," Proc. 44th A. Nat. Forum, American Helicopter Society, Washington, D.C., June, 1988.

3. G.R.Srinivasan, J .D. Baeder, S. Obayashi, and W. J. McCroskey., "Flowfield of a Lifting Rotor in Hover: A Navier-Stokes Simulation," AIAA J., 30, (10), Oct., 1992, pp.2371-2378.

4. Strawn, R. C. and Barth, T. J., "A Finite-Volume Euler Solver for Computing Rotary-Wing Aerodynamics on Unstructured Meshes," J. Am. Helicopter Soc., 38, April, 1993, pp. 61-67.

5. Landgrebe, A. J., "The Wake Geometry of a Hovering Helicopter Rotor and Its Influence on Rotor Performance," J. Am. Helicopter Soc., 17, Oct., 1972, pp. 3-15.

6. Kocurek, J. D. and Tangler, J. L., "A Prescribed Wake Lifting Surface Hover Performance analysis," J. Am. Helicopter Soc., 22, (1), Jan., 1977, pp. 24-35.

7. Clark, D. R. and Leiper, A. C., "The Free Wake Analysis a Method for The Prediction of Helicoper Roter Hovering Performance," J. Am. Helicopter Soc., 15, (1), Jan., 1970, pp. 3-11.

8. Rosen, A. and Grabe, A., "Free Wake Model of Hovering Rotors Having Straight or Curved Blades," J. Am. Helicopter Soc., 33, (3), July, 1988, pp. 11-19.

9. Bagai, A., Leishman, J.G., "Rotor Free-Wake Modeling using a Relaxation Technique - Including Comparisons with Experimental Data," J. Am. Helicopter Soc., 40, (2), April, 1995, pp. 29-41.

10. Scully, M.P., "Computation of Helicopter Rotor Wake Geometry and Its Influence on Rotor Harmonic Airloads," MIT ASRL TR 178-1,March, 1975.

11. Morino, L., Kaprielian, Z. and Sipcic, S. R., "Free Wake Analysis of Helicopter Rotors," Pro. 9th Eur. Rotorcraft Forum, Stresa, Italy, Sept., 1983, Paper No. 3.

12. Katz, J. and Maskew, B., "Unsteady Low-Speed Aerodynamic model for Complete Aircraft Configurations," J. Aircraft, 25, (4), 302-310, 1987.

13. Caradonna, F., Hendley, E., Silva, M., Huang, S., Komerath, N., Reddy, U., Mahalingam, R., Funk, R., Ames R., Darden, L., Villareal, L., Gregory, and Wong, O.,"An Experimental Study of a Rotor In Axial Flight," AHS Specialists' Meeting on Aerodynamics and Aeroacoustics, Williamsburg, VA, Oct. 1997.

14. Rohit, J., A.T. Conlisk, Raghav, M. and N.M. Komerath, "Interaction of Tip-Vortices in the Wake of a Two-Bladed Rotor," AHS 54th Annual Forum, Washington, DC, May 20-22, 1998, pp.182-196.

15. D. J. Lee and S. U. Na, "Predictions of Helicopter Wake Geometry and Air Loadings by using a Time Marching Free Wake Method," Proc. 1st Forum Russian Helicopter Soc., Moscow, Russia, 1994, pp. 69-85.

16. D. J. Lee and S. U. Na, "High Resolution Free Vortex Blob Method for Highly Distorted Vortex Wake Generated from a Slowly Starting Rotor Blade in Hover," Pro. 21th Euro. Rotorcraft Forum, Paper No. II-5, Saint-Petersburg, Russia, 1995.

17. S. U. Na and D. J. Lee, "Numerical Simulations of Wake Structure Generated by Rotating Blades Using a Time Marching Free Vortex Blob Method," European Journal of Mechanics, vol.17, 1998.

18. K. W. Ryu and D. J. Lee, "Sound Radiation from Elliptic Vortex Rings: Evolution and Interaction," Journal of Sound and Vibration, Vol. 200, No. 3, 1997, pp. 281-301.

19. Moore, D.W., "Finite amplitude waves on aircraft trailing vortices," Aeronautical Quarterly, Vol. 23, pp. 307-314, 1972

20. Rosenhead, L, "The spread of vorticity in the wake behind a cylinder," Proc. Roy. Soc., A127, pp.590-612, 1930

21. Leishman, J.G. and Bagai, A., "Challenges in Understanding the Vortex Dynamics of Helicopter Rotor Wake," AIAA-96-1957, 27th AIAA Fluid Dynamics Conference, June 17-20, 1996, New Orleans, LA.